Effect of temperature on the healing capacity and mechanical properties of Ti_2AlC MAX phase ceramics

Suh, Minji; Lee, Dong Heon; Sloof, Willem G.; Lee, Kee Sung

DOI
10.1111/ijac.14704

Publication date
2024

Document Version
Final published version

Published in
International Journal of Applied Ceramic Technology

Received: 12 September 2023 | Revised: 6 December 2023 | Accepted: 2 January 2024

DOI: 10.1111/ijac.14704

International Journal of Applied Ceramic Technology

SPECIAL ISSUE ARTICLE

Effect of temperature on the healing capacity and mechanical properties of Ti_2AlC MAX phase ceramics

Minji Suh[1] | **Dong Heon Lee**[2] | **Willem G. Sloof**[3] | **Kee Sung Lee**[1]

[1]School of Mechanical Engineering, Kookmin University, Seoul, South Korea

[2]Department of Automotive Engineering, Kookmin University, Seoul, South Korea

[3]Department of Materials Science and Engineering, Delft University of Technology, Delft, Netherlands

Correspondence
Kee Sung Lee, School of Mechanical Engineering, Kookmin University, Seoul 02707, South Korea.
Email: keeslee@kookmin.ac.kr

Abstract

In this study, the self-healing capacity of Titanium Aluminum Carbide (Ti_2AlC, MAX phase) was investigated. Bulk coin samples were fabricated to evaluate the self-healing capacity at different temperatures (1000, 1200, and 1400°C). The extensive self-healing capacity of Ti_2AlC was confirmed on larger quasiplastic damage (diameter ≥1 mm) and radial cracks by covering and filling of oxides such as titanium oxide, aluminum oxide, and aluminum titanate oxide. Although the mechanical properties of Ti_2AlC after healing are similar or improved relative to the Ti_2AlC before healing at the microscale, some properties of Ti_2AlC after introducing larger damage and healing at 1400°C showed reduced values due to excessive oxide formation on the surface. For example, the strength of Ti_2AlC healed at 1400°C exhibited 151.4 MPa, which is relative to the original strength of 298.3 MPa. Alternatively, the mechanical properties such as strength, hardness, toughness, and relative modulus of elasticity of Ti_2AlC healed at 1000 or 1200°C and were restored to their original strength after healing. These findings suggest that Ti_2AlC can be used as a healing agent for high-temperature applications, such as environmental barrier coating for gas turbine hot-gas components.

KEYWORDS

cracks/cracking, damage healing, indentation, MAX phase, mechanical properties

1 | INTRODUCTION

Environmental barrier coating (EBC) is used to protect the submaterial of hot gas parts in gas turbines from external environments such as oxygen and water vapor.[1–4] In addition, EBC can protect the submaterial from high temperatures, similar to a thermal barrier coating, which enhances the energy efficiency of the turbine system. This efficiency is a critical factor in the performance of gas turbine engines. The inlet temperature of gas turbine engines is continuously increased from 1000°C up to 1400°C, allowing for maximum combustion efficiency in high-temperature and high-pressure operating conditions.

Recently, fiber-reinforced ceramic composites such as silicon carbide–silicon carbide (SiC–SiC) composites have been applied to hot gas parts of a gas turbine because of their ability to improve the operation temperature and combustion efficiency. This is achieved because of the insulation property of heat and the high oxidation resistance of the composite.[5,6] However, the SiO_2 oxide layer on the surface of SiC–SiC composites can react with water vapor in a high-temperature combustion environment, leading to mass loss and serious damage to turbine components.[3,7,8] In addition, when this composite is used in an aircraft engine, inorganic components known as calcium–magnesium–aluminosilicate (CMAS) with low

melting points can be inhaled through the inlet of an engine from dust, deteriorating the performance of the engine.[9–11] Environmental damages can be prevented by applying EBC on the surface of the SiC–SiC composite to protect it from hot corrosion and fine dust, thereby overcoming the fatal disadvantages.

However, when the EBC is repeatedly exposed to high temperature and cooling conditions of the turbine system, the coating material experiences thermal stress that exceeds the acceptable limit. As a result, damage and cracks can be generated in the coating layer due to the difference in the thermal expansion coefficient between the coating and sublayer. Ultimately, this results in the delamination of the coating layer, which undermines its intended purpose of protecting the composite against oxygen and water vapor at high temperatures. Therefore, ongoing research is focused not only on improving the crack healing performance of the EBC but also on developing self-healing technology that can administer a healing agent to the EBC during turbine operation is in progress to solve this problem.[12–15]

The MAX phase is a terminology that refers to ternary carbide based on $M_{n+1}AX_n$, where $n = 1$ to 3 are possible. When the MAX phase is exposed to air in a high-temperature environment, the oxides formed on the surface fill and expand in the crack, thereby facilitating autonomous crack healing.[16–18] Since Ti_2AlC has no significant difference in thermal expansion coefficient with EBC, we selected it for this study as a healing material among the MAX phases. Titanium oxide (TiO_2) and aluminum oxide (Al_2O_3), which are formed from Ti_2AlC, are oxides with a melting point of over 1500°C. In addition, Ti_2AlC has been reported as a material capable of repeatedly repairing cracks, even under multiple thermal cycles at high temperatures, unlike other crack-healing materials. Our previous study reported that crack healing occurred repeatedly when the thermal cycle was repeated. The mechanical properties such as strength and fracture toughness recover to the original strength.[18]

Most of the research on crack healing has focused on microcracks. For example, radial cracks were generated at the tip of an indenter by inducing plastic damage on the surface of the material using a Vickers or a Knoop indenter. Subsequently, crack healing was examined through post-heat treatment.[12–19] However, not only plastic damage could occur on the surface of the material but also elastic/plastic damage during application. [20–24] Even ceramics with high rigidity and strength exhibit localized ductility, which distinguishes their characteristics from metals and is referred to as "quasi-ductile." The material with a heterogeneous microstructure consisting of elongated grains exhibits shear fault damage with wing cracks at their ends in the subsurface during indentation using a tungsten carbide (WC) sphere. These wing cracks compose the damages, resulting in a quasi-plastic region on the surface.[25] In addition, radial cracks can develop from quasi-plastic damage at higher loads that exceed the critical or fatigue load at a critical number of cycles. If subjected to repeated stress such as fatigue, the micrometer-sized wing cracks can coalesce to develop into large radial cracks.[25,26] Although small microcracks may occur for various reasons when operating a turbine engine, foreign object damage can develop due to collisions with particulates. The type and size of these damages are almost similar to those caused by the indentation test with a spherical indenter.[20,24,26] The quasiductile behavior of MAX phases has been reported for titanium silicon carbide (Ti_3SiC_2) material using indentation with a WC sphere. The damage behavior of the Ti_3SiC_2 MAX phase indicates a quasi-plastic zone composed of microcracks caused by shear stress, instead of the typical cone cracks seen in brittle ceramics.[27]

However, few studies have been conducted on the healing of damage caused by spherical indentation. Our group recently conducted a study on the healing of an indented damaged area.[28,29] The result of our research on the healing of the quasiplastic region of Ti_2AlC indicated that the quasiplastic region with a diameter of 1 mm or more was filled with newly formed oxide, even within a short time of 2 h at a temperature of 1000°C. In addition, the radial cracks near the damage zone healed. Thus, the extensive healing ability of Ti_2AlC was demonstrated. However, further research on the healing process at higher temperatures for quasiplastic damage has not been reported.

Therefore, this study investigated the effect of temperature on the damage-healing abilities of Ti_2AlC as a potential healing agent for the EBC of a turbine engine. The healing temperature was changed at 1000, 1200, and 1400°C, considering the various operating temperatures of the turbine engine, and the effect of temperature was examined. Specifically, we investigated the restoration capacity of mechanical properties after damage healing. We examined the changes in strength, hardness, and toughness after changing the healing temperature conditions to 1000, 1200, and 1400°C. In addition, mechanical behavior such as damage characteristics and the indentation load-displacement curve using a spherical indenter were observed after the healing process. Healing patterns were observed using both optical and digital microscopes, revealing damaged fill and oxide formation.

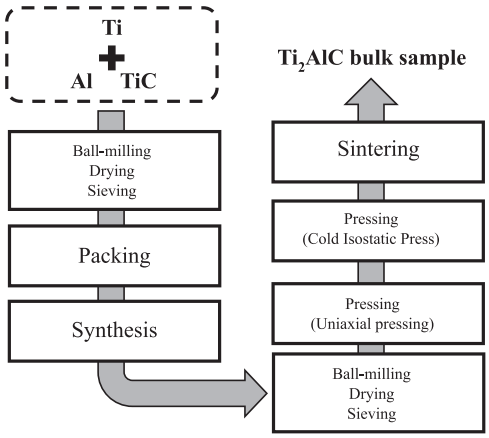

FIGURE 1 Ti_2AlC manufacturing process.

2 | EXPERIMENTAL METHODS

2.1 | Preparation of sample

The manufacturing process of Ti_2AlC is summarized in Figure 1. First, titanium aluminum carbide (Ti_2AlC, 211 MAX phase) powder was synthesized from titanium powder (Ti, 99.5%, 5 μm, US Research Nanomaterials, Inc.), aluminum powder (Al, 99.5%, 3 μm, Kojundo Chemical Laboratory Co. Ltd.), and titanium carbide powder (TiC, 99.5%, 2–5 μm, Kojundo Chemical Laboratory Co. Ltd.) to fabricate a Ti_2AlC coin sample. The powder was prepared by mixing at a molar ratio of 1.15: 1.1: 0.85 for each powder. Acetone was used as a solvent in the prepared powder, and wet ball milling was performed at a speed of 20 rpm for 24 h in a polyethylene container with zirconia (ZrO_2) balls with a diameter of 6 mm. After the wet ball milling process, zirconia balls were removed from the solvent and dried at room temperature for 24 h in a fume hood. After drying, granulated powders were prepared by sieving separation using a 60 μm sieve. Ti_2AlC synthesized powder was obtained by heat-treating in a temperature range of 1350–1500°C for 10–20 h in an argon atmosphere. Synthesized Ti_2AlC was pulverized in a planetary ball mill (Pulverisette 6, Fritsch Co., Ltd.) at 160 rpm, sieved, and then ball milled again for 24 h. After the synthesized powder preparation was completed, uniaxial pressing was performed at 50 MPa using a mold with a diameter of 1 inch (25.4 mm) to form the disk shape, and cold isostatic press (SCIP-50/150, Samyang Ceratech Co., Ltd.) was performed at a pressure of 200 MPa. Some powders were also pressed under the same conditions using a 40 × 40 mm mold with a rectangular shape to fabricate bulk samples for strength measurement. The green bodies were then sintered for 2–10 h by heat treatment in an argon atmosphere in the range of 1450–1640°C.

2.2 | Characterizations

The densities of the Ti_2AlC sintered samples were measured using the Archimedes principle. The surface of the bulk sample was polished to evaluate the mechanical properties and observe the surface. A polishing machine (AutoMet 250, Buehler Co., Ltd.) was used in the order of 25, 16, 9, 6, 3, and 1 μm using diamond paste.

Healing experiments were performed through heat treatment in the air. The heat treatment was performed at 1000, 1200, and 1400°C for 2 h under the condition of a heating rate of 5°C/min.

Vickers indentation was performed on the polished surface of the Ti_2AlC bulk sample. A load of $P = 9.8$ N was applied to the polished surface using a diamond indenter in a Vickers indentation test (MITUTOYO, HM-114) to compare the hardness and toughness before and after crack healing.

In this study, a spherical indentation test method was used to create microcracks and damages on the polished surface of the Ti_2AlC sample, using a universal testing machine (INSTRON, No. 5567). A spherical WC sphere with a radius of $r = 1.98$ mm (J&L Industrial Supply Co.) was attached to a testing machine and increased to a maximum load up to $P = 3000$ N at a constant speed of 0.2 mm/min during loading and unloading. Based on this experiment, the relative hardness and stiffness of the sample were evaluated by analyzing the load-displacement curve graph before and after healing.

A Ti_2AlC strength sample was machined with a dimension of 3 × 4 × 40 mm and chamfering was also performed. We measured the strength of each sample before and after healing at different temperatures. Cracks and damage were induced to the surface of the sample through spherical indentation to conduct a healing test with heat treatment, and the strength before and after healing was compared. At least 5 samples were tested. A spherical WC sphere with a radius of $r = 1.98$ mm (J&L Industrial Supply Co.) was used to create indentation damages and radial cracks. A 4-point bending test was performed in a universal testing machine, and the strength was measured using a jig with specifications of 10 mm upper span and 20 mm lower span. The same speed conditions (0.2 mm/min) as the spherical indentation were used, and the flexural test automatically terminated when a fracture of the sample occurred.

X-ray diffraction (XRD, RINT-2500HF, Rigaku) was performed to identify the healed Ti_2AlC sample. The analysis conditions were set to range from 10° to 80° of diffraction angle, 10 of scan speed, 40 kV and 100 mA of power.

We conducted a microscopic analysis using an optical microscope (GX51, Olympus) and a digital microscope (Smartzoom 5, ZEISS) to observe the pattern of cracks,

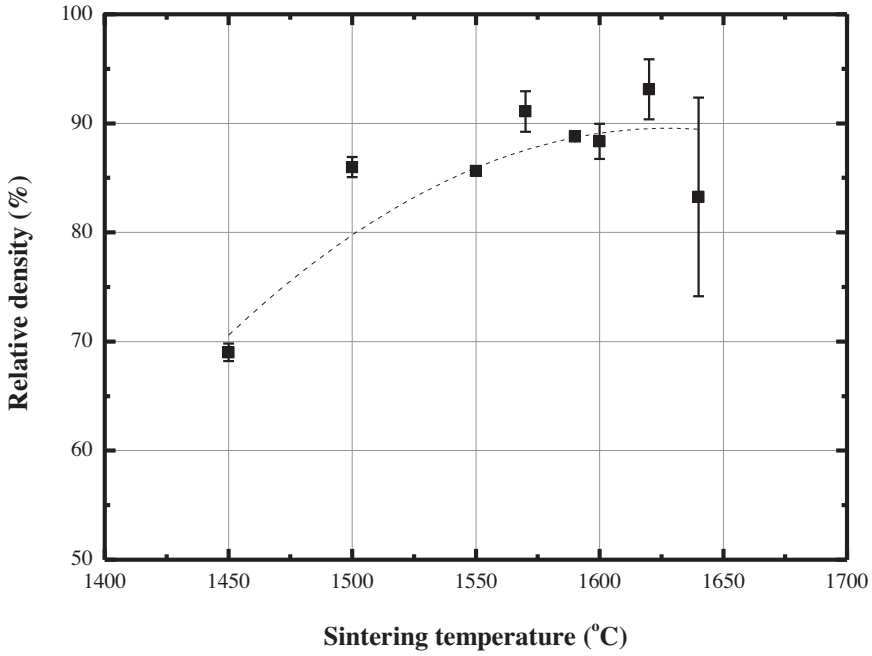

FIGURE 2 Relative densities of Ti_2AlC bulk samples fabricated at different sintering temperatures.

damage, and healed area after heat treatment on the surface of a sample. We also observed the crack, damage, and healed area using a three-dimensional (3D) function of a digital microscope to identify the difference in indentation depth and diameter after healing. Furthermore, scanning electron microscope analysis (SEM, JSM6390, JEOL) was also performed to observe the microstructure before and after healing. In addition, energy dispersive X-ray spectroscopy (EDS) analysis was performed. The composition of the oxide produced through the healing test was analyzed.

3 | RESULTS AND DISCUSSION

The Ti_2AlC powder was successfully synthesized from Ti, Al, and TiC powders. The detailed synthesized results are described in our previous study.[28] The synthesized powder was heat-treated at a higher temperature to produce a sintered sample. Figure 2 shows the results of the relative density of Ti_2AlC sintered at different sintering temperatures. A porous sample with a relative density of approximately 70% was obtained at 1450°C, whereas a relatively dense sintered body with a density of 90% or more was obtained at 1570–1600°C. However, the sintered density decreased at higher temperatures. Therefore, a healing study was performed on the sintered body at 1600–1620°C for 2 h. Hashimoto et al.[30] reported that pressureless sintering can result in Ti_2AlC with a relative density of approximately 92–94%. Zhao et al.[31] obtained a relative density of approximately 90–96% through pressureless sintering of Ti_2AlC. Ping et al.[32] demonstrated that Ti_2AlC can be sintered close to the theoretical density (4.11 g/cm^3) only when pressure is applied during the sintering process, known as pressure sintering.

Damage and cracks were induced using the indentation test method to evaluate the healing capacity of bulk Ti_2AlC material. Figure 3 shows the result of introducing diamond-shaped damage through Vickers indentation, with a load of $P = 9.8$ N applied to the polished surface of the Ti_2AlC bulk material. Figure 3A shows an optical micrograph of the damage formed on the surface after performing Vickers indentation before heat treatment. The microstructure observation indicates that Ti_2AlC, unlike brittle ceramics, contains elongated grains and thus exhibits high toughness. As shown in the figure, the radial cracks do not propagate well and are bent around the indentation damage. The same indentation damage site observed using an optical microscope after heat treatment at 1000°C for 2 h is shown in Figure 3B. New materials that appear bright in color are formed on the surface, as shown in the micrograph. The new materials cover the Vickers indentation damage, indicating healing has occurred. Previous studies have shown that oxides such as TiO_2 and Al_2O_3 are formed on the surface when Ti_2AlC is heat-treated in air.[28,29,33] Figure 3C is an optical micrograph of the damaged area of the same sample with the same load of $P = 9.8$ N and heat treatment at the same temperature, 1000°C, but at a different site of the surface. This micrograph indicates that crack healing occurs by covering oxides at the tip vicinities of the diamond-shaped indentation damage. Healing occurs in the order in which the radial cracks formed on the surface are first filled, and then the oxides are filled into irreversible plastic deformation.

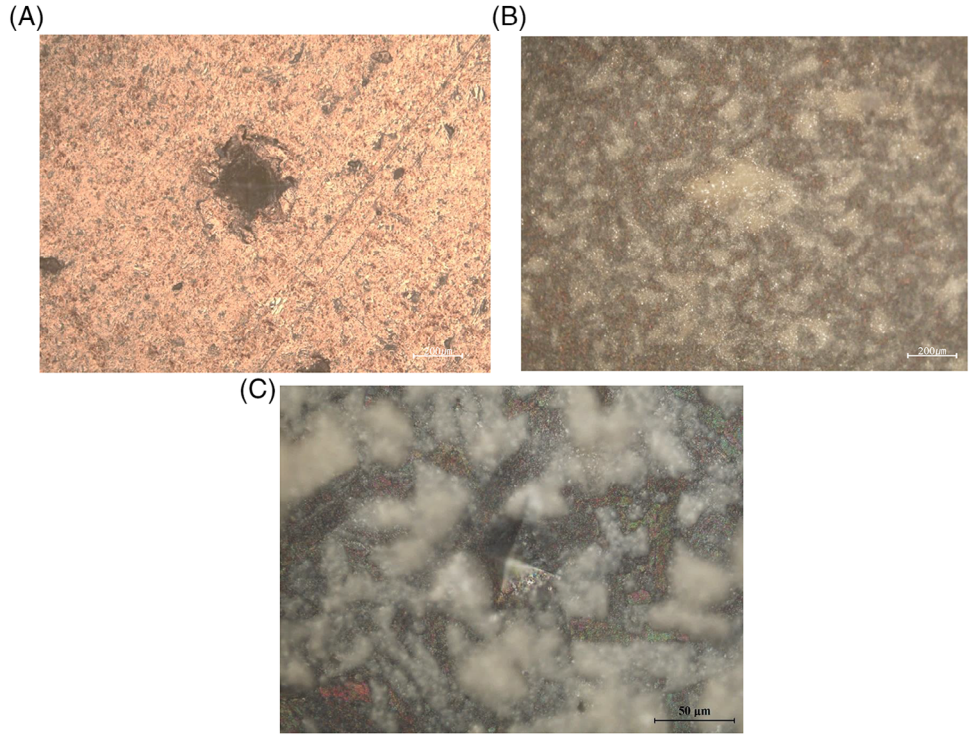

FIGURE 3 Optical micrographs of Vickers indentation damage on the surface of Ti_2AlC sintered sample (A) before and (B) after healing at 1000°C for 2 h in air. (C) shows the oxide formation and healing near the indentation site.

The digital micrographs of Ti_2AlC before and after healing of relatively large damage introduced using a spherical ball instead of a Vickers indenter are shown in Figure 4. A spherical indentation test was performed using a WC sphere with a radius of $r = 1.98$ mm at a load of $P = 3000$ N to produce damage with a diameter of more than 1 mm. The material was pushed outward by the indentation load as the spherical indenter contacted the flat surface of the sample, forming tensile stress near the surface and shear stress in the subsurface.[34] The damages developed above the critical load, causing quasiplastic deformation and radial microcracks. An enlarged optical micrograph was inserted (Figure 4A), showing microcracks formed around the indentation damage due to shear stress acting on the Ti_2AlC with coarse and elongated grains. The heat treatment was performed in air at varied temperatures, 1000, 1200, and 1400°C for 2 h (Figures 4B, D, and F) relative to the micrographs of the Ti_2AlC before heat treatment shown in Figures 4A, C, and E, respectively. The micrographs show that not only indentation damage but also radial microcracks healed with increased oxides on the surface, regardless of the healing temperature. The healing behavior was evident at higher temperatures, where there was increased oxide material accumulation. Thus, the Ti_2AlC MAX phase exhibited an extensive capacity to heal both radial cracks and large quasiplastic deformation at higher temperatures of 1000, 1200, and 1400°C. Preferential oxidation is believed to occur at the damaged site because the site is not faceted but rounded, and the newly formed oxide can diffuse easily into the rounded surface during healing.[35,36] Therefore, extensive damage healing of Ti_2AlC MAX phase ceramics occurs because of high-temperature oxidation.

TABLE 1 Thickness of oxide layer after healing at different temperatures: (A) 1000, (B) 1200, and (C) 1400°C for 2 h in air.

Healing temperature			
Thickness of oxide layer in average (μm)	1000°C	1200°C	1400°C
	112 μm	350 μm	1320 μm

Figure 5 shows the digital microscope observation of the oxide layer formed on the fractured surface of Ti_2AlC samples (3 × 4 × 30 mm) after damage healing at different heat treatment temperatures, 1000, 1200, and 1400°C for 2 h in air. The measured oxide thicknesses are summarized in Table 1 for each healing temperature. The thickness of the oxide layer increases rapidly, as the heat temperature increases as shown in the pictures and data in the table. The average thickness of the oxide layer is 112 μm at 1000°C, which increased to 350 μm at 1200°C. The oxide thickness further increased to 1320 μm at 1400°C. A relatively thick oxide layer was formed when the heat treatment was performed at a higher temperature.

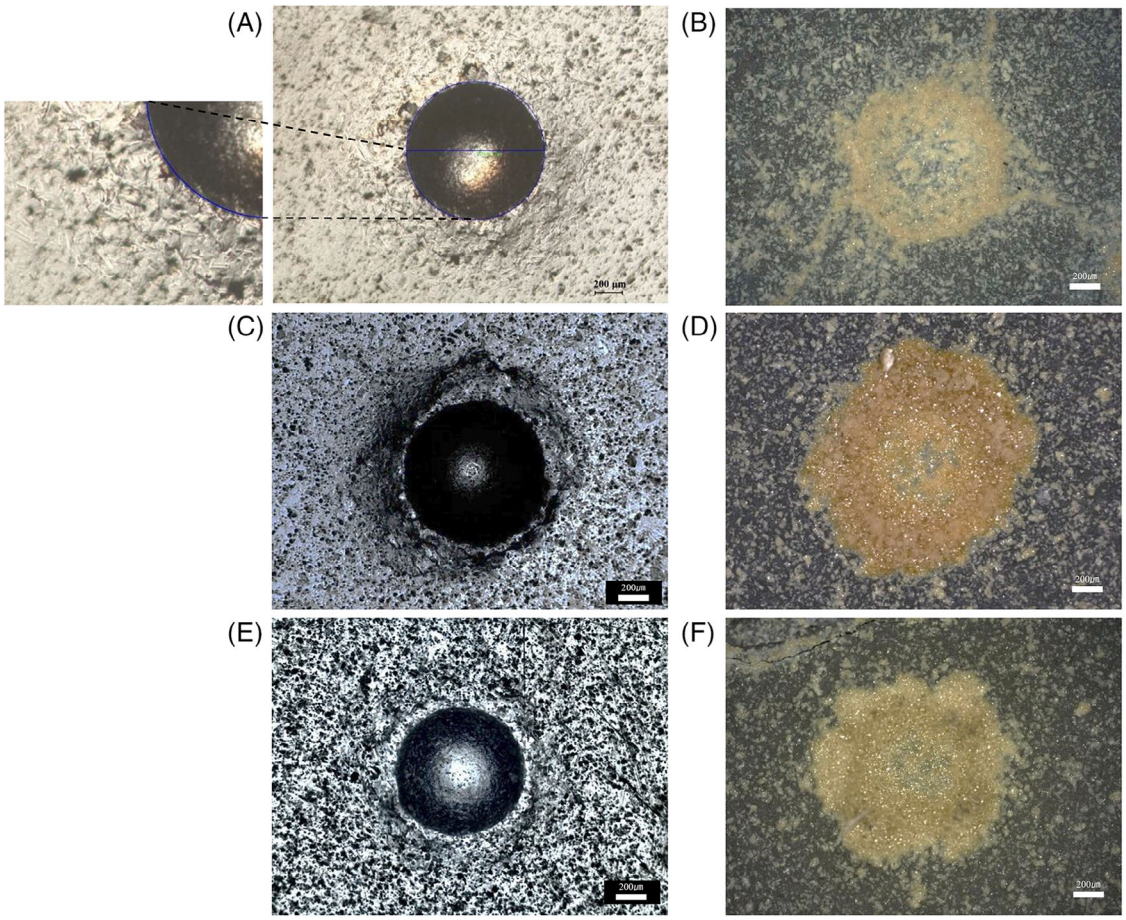

FIGURE 4 Digital micrographs of Ti_2AlC crack and damage: (A) Before healing at 1000°C, (B) after healing at 1000°C, (C) before healing at 1200°C, (D) after healing at 1200°C, (E) before healing at 1400°C, and (F) after healing at 1400°C for 2 h in air after indentation test with a load of 3000N using WC spherical indenter in a radius of 1.98 mm.

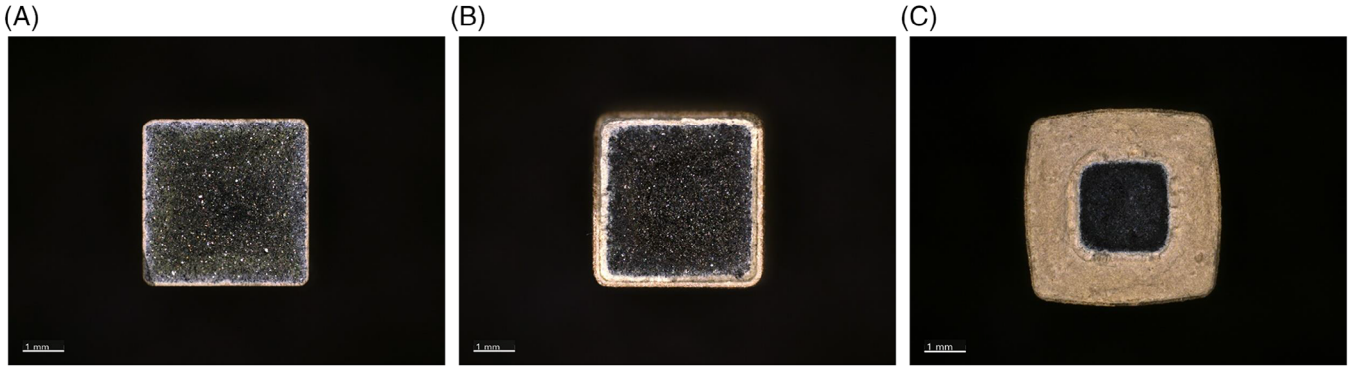

FIGURE 5 Digital micrographs of the fractured surface of Ti_2AlC after healing at different temperatures: (A) 1000°C, (B) 1200°C, and (C) 1400°C for 2 h in air.

Therefore, the damage formed on the surface can be covered and healed by this oxide layer.

The results of measuring the depth of the damaged area of a representative Ti_2AlC undergoing a healing experiment at 1000°C for 2 h were compared with those before healing in Figure 6. Spherical indentation was applied using a WC ball with a radius of 1.98 mm and a load of 3000 N on the surface of Ti_2AlC. The depths of the damages were measured before and after healing at 1000°C using the 3D function of a digital microscope (ZEISS Smartzoom 5). The

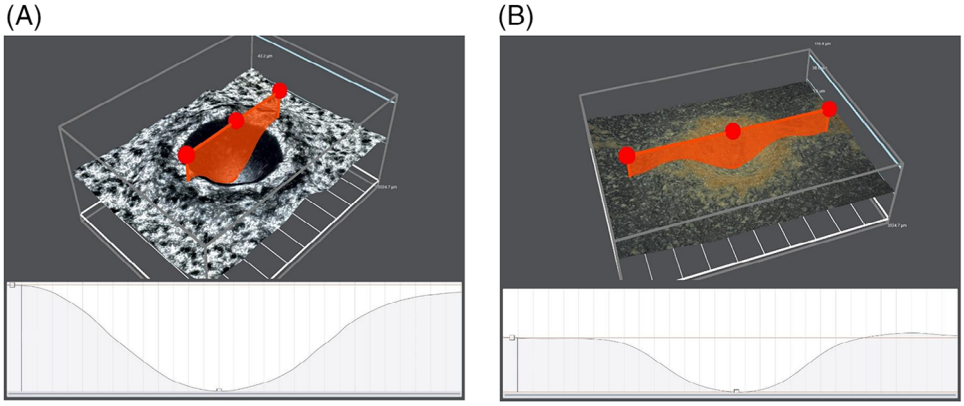

FIGURE 6 Digital micrographs of Ti_2AlC bulk sample using 3D function to measure the indentation depth (A) before healing test and (B) after healing at 1000°C for 2 h in air. The indentation test was performed using WC ball with a radius of 1.98 mm and a load of 3000N.

heights of the damages were measured using the stitching function of the microscope, and an entire 3D-format photograph and depth profile were plotted. Figure 6A shows a representative digital micrograph measuring the indentation depth of quasiplastic damage before the healing experiment. The depth measured at the deepest point of the indentation damage is 84 μm, whereas the depth of quasiplastic damage of the Ti_2AlC MAX phase healed at 1000°C for 2 h is measured as 42 μm. The difference in indentation depth before and after healing decreased. Similarly, the same decrease in the behavior of the indentation depth occurred regardless of healing temperature. Therefore, the oxides formed on the surface (Figure 4) covered and filled the quasi-plastic damage, resulting in a reduction in the damage depth during healing by heat treatment in the air. The surface roughness profiles are shown in the lower part of Figures 6A and B. The surface contour of the roughness after healing is much reduced compared with the depth change before healing.

The representative digital micrographs observing microcracks formed between quasiplastic damages before and after healing at 1000°C of Ti_2AlC MAX phases are shown in Figure 7. The MAX phase exhibiting metallic properties produces irreversible quasiplastic damage due to microcracking by shear faults of elongated grains rather than cracking by brittleness.[27] Even though macrocracks do not appear at lower loads in Ti_2AlC, microcracks can coalesce at higher loads or when repeated fatigue (cyclic) loads are applied.[26] Many literature reports indicate that the strength of the material rapidly reduces when tensile stress is applied to these radial cracks on the surface .[26,37] In this study, the distance between indentation damages was maintained at a narrow interval of 0.6 mm to connect the microcracks generated through the shear fault and the development of radial cracks from quasi-plastic damages during indentation. This was achieved using a WC sphere of r = 1.98 mm at a load of 3000 N. The connected cracks were observed between the two quasiplastic damages using a digital microscope (Figure 7A). Figure 7B shows the digital micrograph observation of the same area after heat treatment at 1000°C for 2 h. The result showed that the connected cracks were healed by filling and covering the crack gaps with the sections of the Ti_2AlC.

The SEM micrographs of the fracture surfaces of Ti_2AlC before and after healing at 1000, 1200, and 1400°C are shown in Figure 8. The fracture surface of a sintered Ti_2AlC without post-heat treatment is shown in Figure 8A. The figure indicates that Ti_2AlC consists of plate-like grains with a layered structure, similar to the microstructure of the conventional MAX phase.[17] Alternatively, Figure 8B–D shows a micrograph of the fracture surface of Ti_2AlC that has undergone healing at 1000, 1200, and 1400°C for 2 h in air, respectively. The grain growth and elongation are not apparent, but some densification occurred by heat treatment at higher temperatures. The entire fracture surface of Ti_2AlC healed at 1400°C was covered with oxide as shown in Figure 8D compared with that shown in Figure 8A. EDS was used to confirm the formation of Ti-based oxide with a grain size of approximately 2–3 μm on the surface, which will be described later. Therefore, the microstructure of the oxide can be ascertained through SEM, acting as a healing agent on the surface and within the cracked gaps. Our previous study analyzed and reported that titanium oxidizes first, followed by aluminum oxidation during the healing of Ti_2AlC. These oxides mutually diffuse to form oxides of titanium on the surface and oxides of aluminum on the subsurface.[33]

The XRD analysis results of each sample's surface, with damage and cracks healed through heat treatment at different temperatures (1000, 1200, and 1400°C) are shown in Figure 9. The XRD result of Ti_2AlC after undergoing the healing experiment at 1000°C for 2 h is shown in Figure 9A. On one hand, healing at high temperatures in

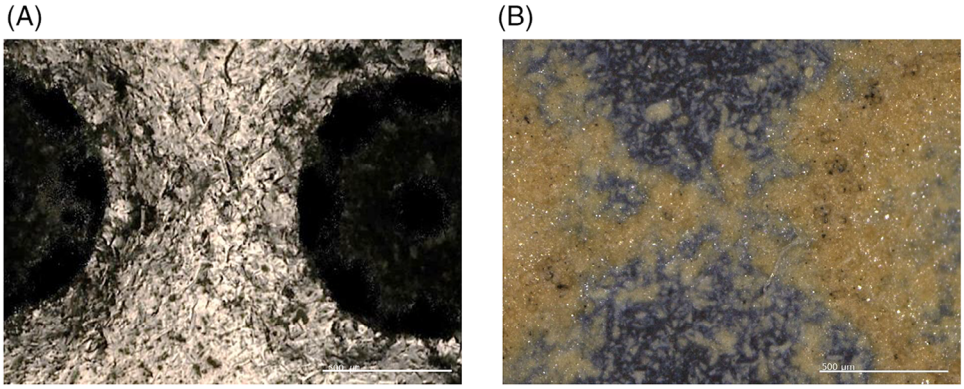

FIGURE 7 Indentation damage and microcracks on Ti_2AlC bulk sample using a WC ball with a radius of 1.98 mm and a load of 3000N. (A) The microcracks between two indentation damage sites coalesced and (B) the oxides filled the radial crack and damages due to heat treatment after healing test at 1000°C for 2 h in the air.

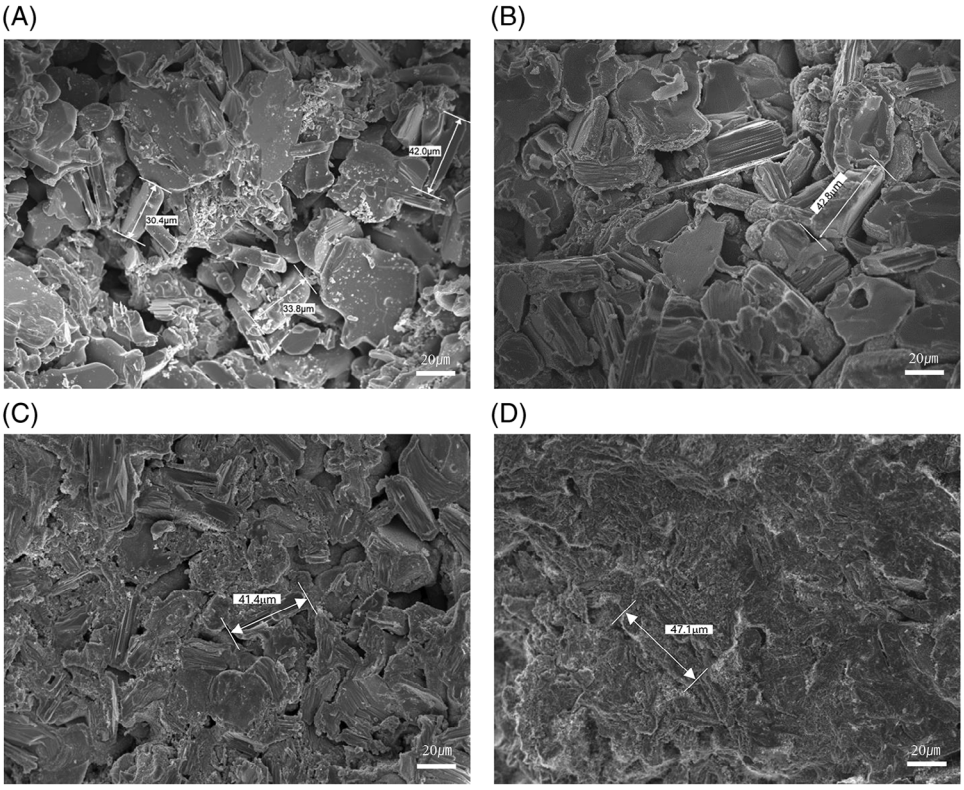

FIGURE 8 SEM micrographs of the fracture surface of Ti_2AlC (A) before healing, (B) after healing at 1000°C, (C) after healing at 1200°C, and (D) after healing at 1400°C for 2 h in air.

air resulted in the formation of TiO_2, a Ti-based oxide, and Al_2O_3, an Al-based oxide, on the surface of Ti_2AlC. On the other hand, TiO_2 was detected at 1000°C, but a new oxide phase of aluminum titanate oxide (Al_2TiO_5) was detected, which had reacted from TiO_2 and Al_2O_3 in the Ti_2AlC under the healing conditions at 1200°C for 2 h (Figure 9B). The XRD result of the Ti_2AlC healed at 1400°C for 2 h is shown in Figure 9C. TiO_2 and Al_2TiO_5 were detected in the same way. Note that Al_2TiO_5 is characterized by high insulation, low thermal conductivity, and excellent thermal shock resistance. In addition, it was reported that the weight loss of Al_2TiO_5 at 1500°C in a water vapor environment was very small[38]. Even though microcracks can be developed because of the low thermal expansion coefficient, Al_2TiO_5 is widely used in the industry as a refractory material owing to its high-temperature

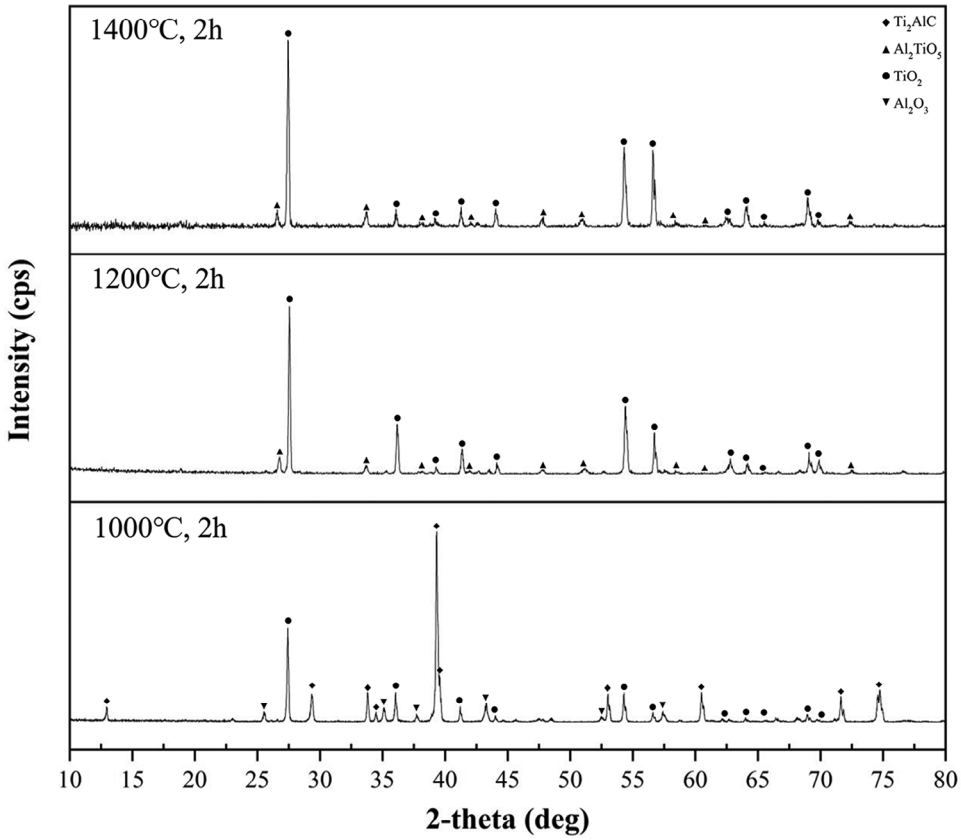

FIGURE 9 XRD analysis results of Ti_2AlC after healing at each different temperatures in air for 2 h.

structural properties, corrosion resistance, and mechanical strength.[39] The XRD analysis results indicate that the Quasi-plastic damage and radial cracks due to spherical indentation can be healed through high-temperature oxidation of Ti_2AlC. When a crack-healing material such as Ti_2AlC MAX phase is added to the EBC and exposed to high temperature in air, the healing agent reacts with oxygen in a high-temperature turbine operating environment to produce Ti and Al-based oxides, which effectively heal damage and cracks. In addition, it can insulate heat and act as an environment-resistant coating material.

An EDS analysis was performed to analyze components formed on the Ti_2AlC surface after healing. The surface analysis results of the Ti_2AlC subjected to the healing at 1400°C for 2 h are shown in Figure 10. The cross-section of the Ti_2AlC after healing by heat treatment, where the indentation damage was filled with oxides, was analyzed. Oxygen elements were detected with the components of Ti, Al, and C in the filled phase on the surface damage, as shown in the figure. This detection was similar regardless of the heat treatment temperature. Specifically, the oxygen element was evenly distributed in the area where the indentation damage had healed. As the oxide layer was thicker at higher healing temperatures (Table 1), more oxygen was detected at higher healing temperatures through analysis.

As a result, the oxides formed during Ti_2AlC healing at high temperatures filled the indentation damage on the surface and through the cross-section. XRD and EDS analysis of Ti_2AlC healed at 1000–1400°C for 2 h confirmed the presence of TiO_2, Al_2O_3, and Al_2TiO_5 oxides (Figures 9 and 10), indicating that these oxides play a significant role in healing the damage and cracks of the material.

Generally, brittle materials, such as ceramics, exhibit elastic behavior above a critical load during spherical indentation tests, and cracks begin to form around the indentation area, leading to a reduction in material strength. Even in the case of high-tough materials, such as the MAX phase, quasiplastic damages, including microcracks, also contribute to decreased strength.[37] Moreover, the strength of quasiplastic damages can be significantly reduced, particularly when microcracks coalesce and expand into large radial cracks.[26] Several studies have been conducted on strength recovery through the healing of cracks.[13,19,28,33] We recently conducted a healing study on quasiplastic damage with a diameter of 1 mm or more and found that mechanical strengths are recovered through heat treatment on the damage.[29]

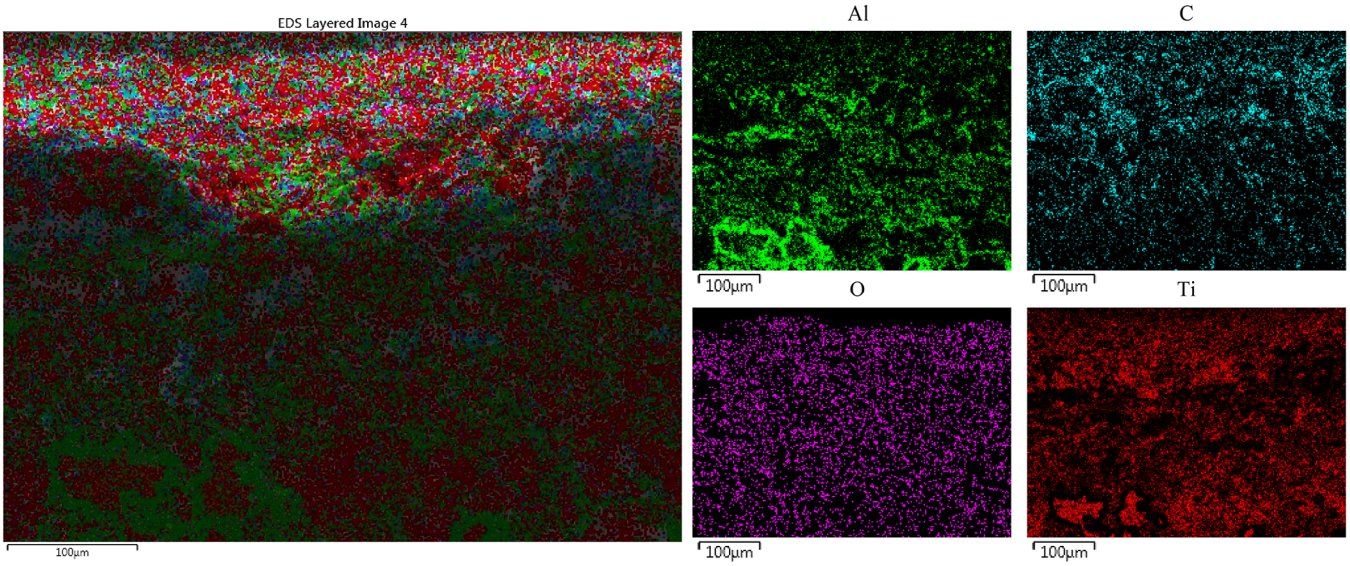

FIGURE 10 EDS images of Ti_2AlC sample after healing at 1400°C for 2 h in air.

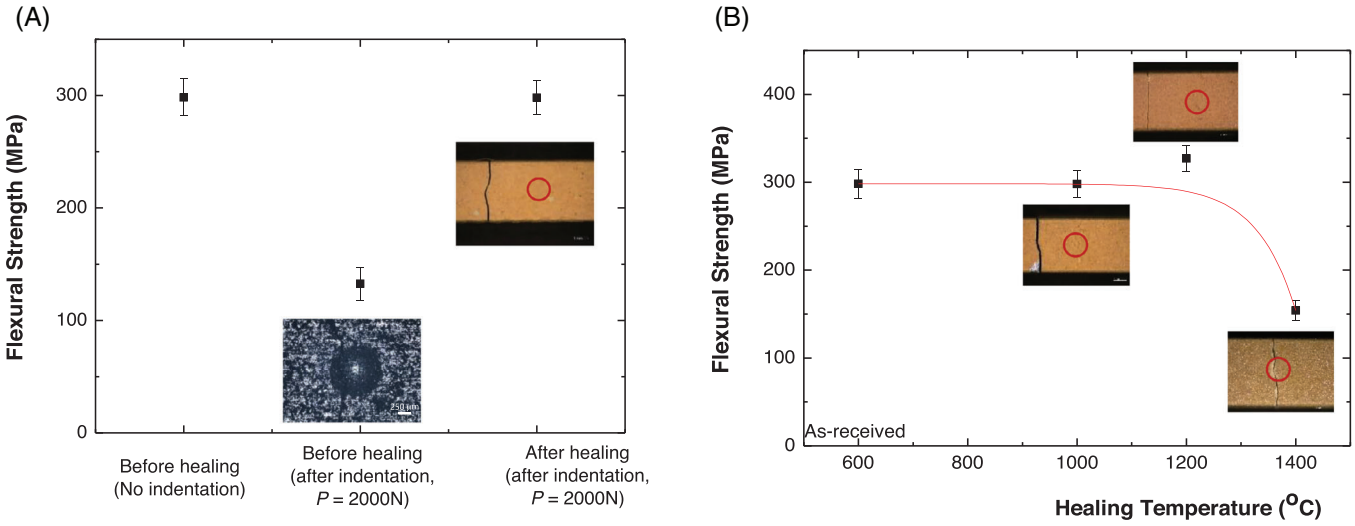

FIGURE 11 (A) Four-point bending test results of the original Ti_2AlC bar sample, the sample containing quasi-plastic damage and the sample containing the damage and posthealed. (B) Four-point bending test results before and after healing at each different temperature for 2 h.

The 4-point flexural strength results before and after heat treatment at 1000°C are shown in Figure 11A. The strength after introducing quasi-plastic damage to the surface by applying a load of $P = 300$ N with a radius of $r = 1.98$ mm, without heat treatment is also included in the graph. The original strength of 298.3 ± 16.4 MPa was reduced to 132.6 ± 14.5 MPa because of the quasi-plastic surface formed on the surfaces (55.6% of strength loss occurred). However, the strength value recovered to 298.0 ± 15.2 MPa when healing was performed on the quasi-plastic damage at a temperature of 1000°C for 2 h in air. The graph also includes optical micrographs indicating the fracture origin after the strength test. While the fracture occurred through quasiplastic damage in the sample without heat treatment, all the fractures happened outside of the damaged area in the sample with healing, indicating that the indentation damage or the microcracks in the damaged area were completely healed, causing the failure to occur outside of the damaged site.

The 4-point flexural strengths of the Ti_2AlC heat-treated at different temperatures, (1000, 1200, and 1400°C) for 2 h were compared with that of the Ti_2AlC before healing (Figure 11B). The mean strength of Ti_2AlC before healing was 298.3 ± 16.4 MPa, whereas that of Ti_2AlC after

healing the quasiplastic damage on the surface at 1000°C was 298.0 ± 15.2 MPa. When the spherical indentation test was performed on the Ti_2AlC at load $P = 300$ N using a WC sphere with a radius of $r = 1.98$ mm and then heat-treated at 1000°C, a recovery rate of 99.9% compared with the initial strength was observed. Moreover, the strength of the Ti_2AlC sample heat-treated at 1200°C increased to 326.9 ± 14.9 MPa compared with the original strength. However, the strength of the Ti_2AlC sample healed at 1400°C was relatively low at 154.1 ± 11.7 MPa compared with those of the Ti_2AlC sample heat-treated at 1000°C or 1200°C. Excessive oxidation on the surface of the sample and increased amount of Al_2TiO_5 phase due to heat treatment at 1400°C can decrease damage strength. The oxidation into the Al_2TiO_5 phase caused a significant thermal expansion mismatch, creating new microcracks. These microcracks can propagate to large cracks during oxidation, ultimately causing fracture, as shown in the inserted optical micrograph in Figure 11B. Fracture occurred outside the damaged site when heat treatment was performed at 1000°C and 1200°C whereas all the fracture through the damage was occurred at 1400°C. This result indicates that quasiplastic damage zones comprising microcracks were the main cause of fracture during the strength test. However, the Ti_2AlC material exhibited excellent strength restoration and good damage tolerance properties because of its damage healing capacity at 1000 and 1200°C. The optimal temperature for restoring strength through healing is less than 1400°C, and the mechanical strength is preserved at these temperatures. Further study is being conducted to reduce oxide thickness at 1400°C.

Vickers indentation characterization was performed on polished Ti_2AlC before and after healing at 1000, 1200, and 1400°C through heat treatment. The hardness and toughness of the Ti_2AlC were plotted (Figure 12) to analyze the effect of healing at high temperatures.

The hardness exhibited similar or increased values when characterized by microindenter after changing from MAX carbide to oxides such as TiO_2, Al_2O_3, and Al_2TiO_5 on the surface (Figure 12A) during healing. The hardness of Ti_2AlC before healing was 2.3 ± 0.4 GPa on average and increased to 3.5 ± 1.3 GPa when heat treatment was performed at 1000°C for 2 h. Healing at 1200°C increased the hardness value by an average of 4.1 ± 0.8 GPa and healing at 1400°C increased the hardness value by an average of 5.0 ± 1.3 GPa. The microhardness value increased more than twice after healing.

Figure 12B plots a graph comparing the fracture toughness before healing with the toughness after healing at each temperature. The initial fracture toughness before healing of the Ti_2AlC was measured at an average of 4.4 ± 0.9 $MPa{\cdot}m^{1/2}$ using Vickers indentation. After healing at 1000°C for 2 h, the average fracture toughness increased to 4.8 ± 0.8 $MPa{\cdot}m^{1/2}$ and maintained at 4.8 ± 0.7 $MPa{\cdot}m^{1/2}$ after healing at 1200°C. The fracture toughness further increased to 5.2 ± 0.5 $MPa{\cdot}m^{1/2}$.

Thus, the hardness and toughness increase in the microscale area is due to healing through heat treatment even though the indentations were performed on the oxide surface. The increase in hardness and toughness in the microscale area is due to the formation of Al_2O_3, which has better mechanical properties[29,33] than Ti_2AlC, and the formation of Al_2TiO_5 oxide at temperatures above 1200°C.[39]

However, when the size of the indentation damaged area is larger than that of the Vickers indentation and the load is increased, the relative hardness and elastic modulus measured by the spherical indentation test using a WC sphere tend to slightly decrease as the heat treatment temperature increases. The schematic of the spherical indentation is shown in Figure 13A. Figure 13B plots the indentation load-displacement curve of Ti_2AlC during spherical indentation before and after healing at different temperatures (1000, 1200, and 1400°C). When the obtained indentation load-displacement curves were compared, the Ti_2AlC heat-treated at 1000°C exhibited the most elastic behavior, and the compression strain increased as the heat temperature increased. Alternatively, the loading curve of Ti_2AlC healed at 1400°C exhibited an indentation load drop at 1600 N. This seems to be a fracture phenomenon caused by Al_2TiO_5 in the oxide formed due to heat treatment at 1400°C.

Table 2 compares the relative hardness and elastic modulus of the residual displacement of Ti_2AlC after unloading and the slope of the loading or unloading curve of Ti_2AlC heat-treated at different temperatures. The residual displacement after unloading is closely related to the hardness of the material, and the slope of the curve during loading or unloading is related to the elastic modulus.[28,29] In the case of residual displacement, the Ti_2AlC heat-treated at 1000°C exhibited a similar relative hardness of 82.4% compared with the displacement data of the sample before healing, which we set 100%. However, in the case of the Ti_2AlC heat-treated at 1400°C, a significant change in relative hardness of 45% was observed compared with the data before healing. Nonetheless, the relative modulus of elasticity, obtained from the slope of the curve, did not change significantly (92.4–101.2% in the Table 2), except for a slight decrease during loading (74.6%) at higher heat treatment temperatures.

Therefore, although the mechanical properties such as hardness and toughness tend to increase with heat-treatment temperature due to the oxide with high mechanical properties from the viewpoint of the microscale of the Ti_2AlC, the hardness and elastic modulus tend to decrease

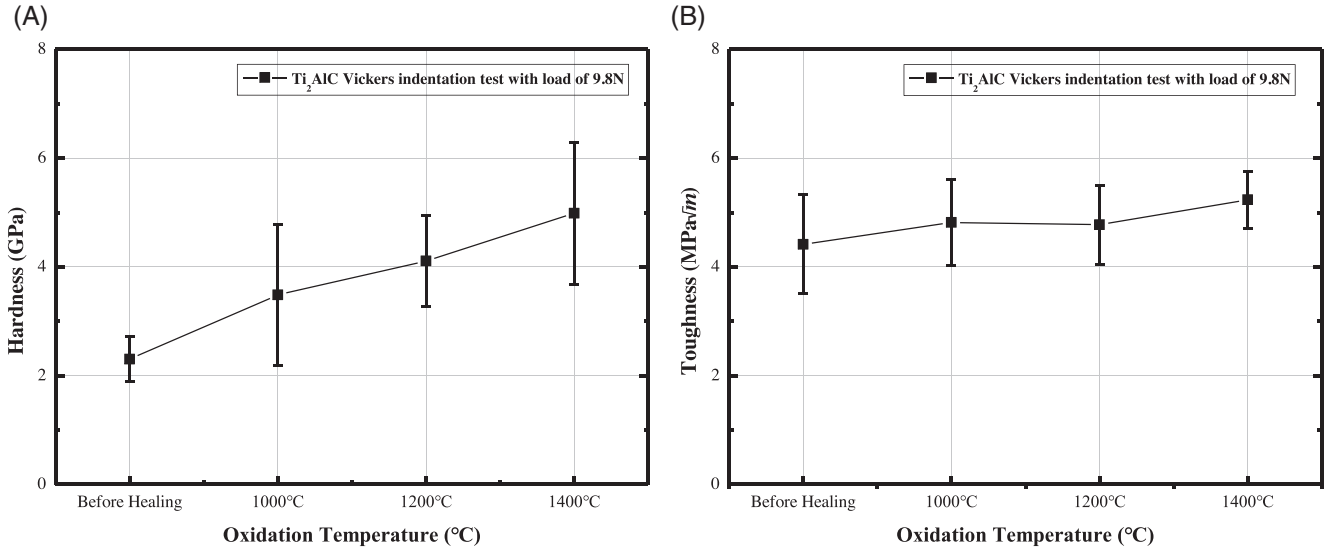

FIGURE 12 (A) Vickers hardness and (B) fracture toughness results with a load of $P = 9.8$N on Ti_2AlC bulk samples after healing at 1000, 1200, and 1400°C for 2 h in air. The graph also includes the data of Ti_2AlC bulk samples before healing.

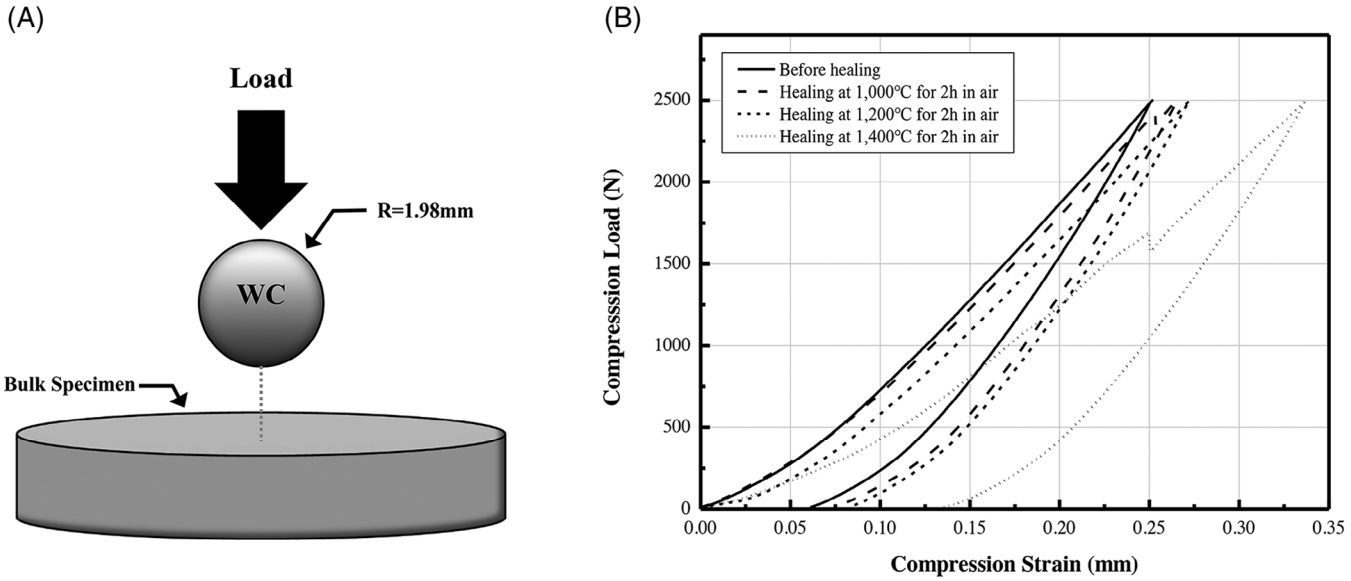

FIGURE 13 (A) Schematic of spherical indentation and (B) indentation load-displacement curves of Ti_2AlC bulk samples with a load of $P = 2500$N using WC spherical indenter in a radius of $r = 1.98$ mm before healing and after healing at 1000, 1200, and 1400°C for 2 h in air.

TABLE 2 Relative hardness and elastic modulus of Ti_2AlC bulk samples with a load of $P = 2500$N using WC spherical indenter in a radius of $r = 1.98$ mm before healing and after healing at 1000, 1200, and 1400°C for 2 h in air.

		Before healing	1000°C	1200°C	1400°C
Relative hardness (from residual displacement)	Residual displacement (mm)	0.0061	0.074	0.082	0.136
	Variance (%)	100	82.4	74.4	44.8
Residual elastic modulus (from slope of curves)	Slope during loading (%)	100	94.6	92.4	74.6
	Slope during unloading (%)	100	101.2	101.2	95.5

somewhat due to relative plastic behavior when characterizing Ti_2AlC using WC spheres, which can produce larger indentation damage (more than 1 mm diameter) than that of Vickers indentation characterization (~several hundreds of micrometers) by size effect.

Nevertheless, the reduction in mechanical properties is not significant when healing at 1000 and 1200°C, thereby allowing for the recovery of the initial mechanical properties through the healing of damage. Therefore, Ti_2AlC can be used as a damage–healing material with excellent mechanical properties at the operating temperature of a gas turbine system.

4 | CONCLUSION

In this study, the effect of temperature of heat treatment on the healing capacity of Ti_2AlC bulk was investigated. We varied the healing temperature 1000, 1200, and 1400°C, respectively, after inducing the quasi-plastic damage. Finally, the mechanical properties such as strength, hardness, toughness, and relative modulus of elasticity were investigated before and after healing.

1. The heat treatment on the Ti_2AlC MAX phase in air produced the oxide on the surface of the sample such as TiO_2, Al_2O_3, and Al_2TiO_5. The entire surface of the sample was covered with oxide during healing in air. Compositional analysis showed that oxygen was evenly distributed in the area where the indentation damage had healed. The oxide thickness increased from 112 μm at 1000°C to 1320 μm at 1400°C during healing on the bar sample (3 × 4 × 30 mm).
2. Healing of damage developed by Vickers or spherical indentation methods was investigated. Spherical indentation using a WC sphere induced a larger size of damage and cracking. However, heat treatment at high temperatures in the air for 2 h successfully healed the damages and radial cracks. The surface damage and radial cracks were extensively covered and filled by newly formed oxide on the surface. The deepest depth of damage before healing was reduced by oxide filling due to preferential oxidation at the rounded site of the damage. The surface profile was also smoothed using the healing process.
3. The mechanical properties of Ti_2AlC healed at 1400°C exhibited lower strength (151.4 MPa relative to initial original strength of 298.3 MPa), lower relative hardness 45% relative to the residual displacement of the Ti_2AlC without healing, 100%) and lower relative modulus of elasticity (74.6 % relative to the slope of load-displacement curve during loading for sample without healing, 100%) due to excessive oxide formation on the surface during healing. On the other hand, the mechanical properties of Ti_2AlC healed at 1000°C and 1200°C are similar to or improved relative to the original strength of Ti_2AlC. While the strength of initial original strength of 298.3 MPa was not reduced by healing at 1000°C (298.0 MPa) and 1200°C (326.9 Pa), the Vickers hardness/toughness rather increased by healing at 1000°C (3.5 GPa/4.8 $MPa{\cdot}m^{1/2}$ relative to 2.3 GPa/4.4 $MPa{\cdot}m^{1/2}$ before healing) and 1200°C (4.1 GPa/4.8 $MPa{\cdot}m^{1/2}$). The relative hardness and elastic modulus after healing at 1000°C and 1200°C were similar to those of Ti_2AlC before healing.

ACKNOWLEDGEMENTS

This study was supported by the IT R&D program of MOTIE/KEIT (no. 20011237, SiC fiber reinforced ceramic composite ceramic coating developed to improve the environmental performance).

CONFLICT OF INTEREST STATEMENT

The authors declare no conflict of interest.

ORCID

Kee Sung Lee https://orcid.org/0000-0002-9658-739X

REFERENCES

1. Lee KN, Water DL, Puleo BJ, Garg A, Jennings WD, Costa G, et al. Development of oxide-based high temperature environmental barrier coatings for ceramic matrix composites via the slurry process. J Eur Ceram Soc. 2021;41:1639-53.
2. Tian J, Zheng L, Li Z, Li J, Wang J. Exploration of the low thermal conductivities of γ-$Y_2Si_2O_7$, β-$Y_2Si_2O_7$, β-$Yb_2Si_2O_7$,and β-$Lu_2Si_2O_7$ as novel environmental barrier coating candidates. J Eur Ceram Soc. 2016;36:2813-23.
3. Ridley MJ, Opila EJ. High-temperature water-vapor reaction mechanism of barium strontium aluminosilicate (BSAS). J Eur Ceram Soc. 2022;42:3305-12.
4. Bakan E, Sohn YJ, Vaβen R. Metastable to stable phase transformation in atmospheric plasma sprayed Yb-silicate coating during post-heat treatment. Scrip Mater. 2023;225:115169.
5. Brewer D. HSR/EPM combustor materials development program. Mater Sci Eng. 1999;261:284-89.
6. Zok FW. Ceramic-matrix composites enable revolutionary gains in turbine engine efficiency. Am Ceram Soc Bull. 2016;95:22-28.
7. Lee KN. Current status of environmental barrier coatings for Si-based ceramics. Surf Coat Technol. 2000;133-134:1-7.
8. Smialek JL, Robinson RC, Opila EJ, FOX DS, Jacobson NS. SiC and Si_3N_4 recession due to SiO_2 scale volatility under combustor condition. Adv Compos Mater. 1999;8:33-45.
9. Ahlborg NL, Zhu D. Calcium-magnesium aluminosilicate (CMAS) reactions and degradation mechanisms of advanced environmental barrier coatings. Surf Coat Technol. 2013;237:79-87.
10. Krämer S, Yang J, Levi CG. Thermochemical interaction of thermal barrier coatings with molten CaO-MgO-Al_2O_3-SiO_2 (CMAS) deposit. J Am Ceram Soc. 2006;89:3167-75.

11. Jang BK, Feng FJ, Suzuta K, Tanaka H, Matsushita Y, Lee KS, et al. Corrosion behavior of volcanic ash and calcium magnesium aluminosilicate on Yb_2SiO_5 environmental barrier coatings. J Ceram Soc Jpn. 2017;125:326-32.
12. Bakan E, Vaβen R. Crack healing mechanism in atmospheric plasma sprayed Yb-silicate coatings during post-process heat treatment. J Eur Ceram Soc. 2023;43:3684-93.
13. Nguyen ST, Nakayama T, Suematsu H, Iwasawa H, Suzuki T, NIhara K. Self-crack healing ability and strength recovery in ytterbium disilicate/silicon carbide nanocomposites. Appl Ceram Technol. 2019;16:39-49.
14. Nozahic F, Estournès C, Carabat AL, Sloof WG, Zwaag S, Monceau D. Self-healing thermal barrier coating systems fabricated by spark plasma sintering. Mater Des. 2018;143:204-13.
15. Kulczyk-Malecka J, Zhang X, Carr J, Carabat AL, Sloof WG, Zwaag S, et al. Influence of embeeded $MoSi_2$ particles on the high temperature thermal conductivity of SPS produced yttra-stabilized zirconia model thermal barrier coating. Surf Coat Technol. 2016;308:31-39.
16. Radovic M, Barsoum MW. Max phases: bridging the gap between metals and ceramics. Am Ceram Soc Bull. 2013;92:20-27.
17. Farle AS, Kwakernaak C, Zwaag S, Sloof WG. A conceptual study into the potential of $M_{n+1}AX_n$-phase ceramics for self-healing of crack damage. J Eur Ceram Soc. 2015;35:37-45.
18. Sloof WG, Pei R, McDonald Fife JL, Shen L, Boatemaa L, Farle AS, et al. Repeated crack healing in MAX-phase ceramics revealed by 4D in situ synchrotron X-ray tomographic microscopy. Sci Rep. 2016;6:23040.
19. Ando K, Furusawa K, Takahashi K, Sato S. Crack-healing ability of structural ceramics and a new methodology to guarantee the structural integrity using the ability and proof-test. J Eur Ceram Soc. 2005;25:549-58.
20. Presby MJ, Mansour R, Manigandan K, Morscher GN, Abdi F, Godines C, et al. Characterization and simulation of foreign object damage in curved and flat SiC/SiC ceramic matrix composites. Ceram Int. 2019;45: 2635-43.
21. Guo J, Zuo H, Zhong Z, Jiang H. Foreign object monitoring method in aero-engines based on electrostatic sensor. Aerosp Sci Technol. 2022;123:107489.
22. Fleck NA, Zisis TH. The erosion of EB-PVD thermal barrier coatings: the competition between mechanisms. Wear. 2010;268:1214-24.
23. Wellman RG, Nicholls JR. Erosion, corrosion and erosion-corrosion of EB PVD thermal barrier coatings. Tribol Int. 2008;41:657-62.
24. Panakarajupally RP, Mirza F, Rassi JE, Morscher GN, Abdi F, Choi S. Solid particle erosion behavior of melt-infiltrated SiC/SiC ceramic matrix composites (CMCs) in a simulated turbine engine environment. Composites Part B. 2021;216:108860.
25. Lawn BR, Padture NP, Cai H, Guiberteau F. Making ceramics "ductile". Science. 1994;263:1114-16.
26. Lee KS, Jung YG, Peterson IM, Lawn BR. Model for cyclic fatigue of quasi-plastic .ceramics in contact with spheres. J Am Ceram Soc. 2000;83:2255-62.
27. Low IM, Lee SK, Lawn BR. Contact damage accumulation in Ti_3SiC_2. J Am Ceram Soc. 1998;81:225-28.
28. Lee GW, Kim TW, Sloof WG, Lee KS. Self-healing capacity of mullite-Yb_2SiO_5 environmental barrier coating material with embedded Ti_2AlC MAX phase particles. Ceram Int. 2021;47:22478-86.
29. Lee KS, Ahn H, Lee GW, Sloof WG. Self-healing of indentation damage in Ti_2AlC MAX phase ceramics. Mater Lett. 2023;334:133683.
30. Hashimoto S, Takeuchi M, Inoue K, Honda S, Awaji H, Fukuda K, et al. Pressureless sintering and mechanical properties of titanium aluminum carbide. Mater Lett. 2008;62:1480-83.
31. Zhao Z, Liu H, Li X, Zhuang Y, Zhang X, Yan Q. Ti_2AlC bulk ceramics produced by gelcasting and Al-rich pressureless sintering. Ceram Inter. 2020;46:14767-75.
32. Ping W, Bing-chu M, Xiao-lin H, Wei-bing Z. Synthesis of Ti_2AlC by hot pressing and its mechanical electrical properties. Trans Nonferros Met Soc China. 2007;17:1001-4.
33. Boatemaa L, Bosch M, Farle AS, Bei GP, Zwaag S, Sloof WG. Autonomous high-temperature healing of surface cracks in Al_2O_3 containing Ti_2AlC particles. J Am Ceram Soc. 2018;101:5684-93.
34. Lawn BR. Indentation of ceramics with spheres: A century after Hertz. J Am Ceram Soc. 1998;81:1977-94.
35. Tavangarian F, Hui D, Li G. Crack-healing in ceramics. Composites Part B. 2018;144:56-87.
36. Choi SY, Kang SJ. Sintering kinetics by structural transition at grain boundaries in barium titanate. Acta Mater. 2004;52:2937-43.
37. Lawn BR, Lee SK, Peterson IM, Wuttiphan S. Model of strength degradation from Hertzian contact damage in tough ceramics. J Am Ceram Soc. 1998;81:1509-20.
38. Ueno S, Jayaseelan D., Kondo N, Ohji T, Kanzaki S. High temperature water vapor corrosion behavior of titanium aluminate (Al_2TiO_5). J Ceram Soc Jpn. 2003:44:860-62.
39. Sarkar N, Lee KS, Park JG, Mazumder S, Aneziris CG, Kim IJ. Mechanical and thermal properties of highly porous Al_2TiO_5-mullite ceramics. Ceram Inter. 2016;42:3548-55.

How to cite this article: Suh M, Lee DH, Sloof WG, Lee KS. Effect of temperature on the healing capacity and mechanical properties of Ti_2AlC MAX phase ceramics. Int J Appl Ceram Technol. 2024;1–14. https://doi.org/10.1111/ijac.14704